

# Implantable Silk Composite Microneedles for Programmable Vaccine Release Kinetics and Enhanced Immunogenicity in Transcutaneous Immunization

Peter C. DeMuth, Younjin Min, Darrell J. Irvine,\* and Paula T. Hammond\*

Microneedle vaccines mimic several aspects of cutaneous pathogen invasion by targeting antigen to skin-resident dendritic cells and triggering local inflammatory responses in the skin, which are correlated with enhanced immune responses. Here, we tested whether control over vaccine delivery kinetics can enhance immunity through further mimicry of kinetic profiles present during natural acute infections. An approach for the fabrication of silk/poly(acrylic acid) (PAA) composite microneedles composed of a silk tip supported on a PAA base is reported. On brief application of microneedle patches to skin, the PAA bases rapidly dissolved to deliver a protein subunit vaccine bolus, while also implanting persistent silk hydrogel depots into the skin for a low-level sustained cutaneous vaccine release over 1–2 weeks. Use of this platform to deliver a model whole-protein vaccine with optimized release kinetics resulted in >10-fold increases in antigen-specific T-cell and humoral immune responses relative to traditional parenteral needle-based immunization.

compared with traditional parenteral immunization approaches targeting less immunogenic tissues such as muscle (reviewed elsewhere).<sup>[1]</sup> Microneedle vaccination has in many cases also outperformed hypodermic needle-based delivery to the skin, suggesting the importance of factors relating to microneedle delivery itself, such as the inflammatory state generated by micrometer-scale wounding following microneedle insertion.<sup>[2,3]</sup> Unrelated studies have begun to reveal the importance of antigen and adjuvant delivery kinetics in the developing immune response, both within the context of vaccination and in natural responses to infection.<sup>[4–7]</sup> For example, the magnitude, functionality, and phenotype of CD8+ T-cell responses can be shaped by immunizations where antigen or adjuvant delivery kinetics are controlled over

## 1. Introduction

Microneedle skin patches represent an attractive technology for non-invasive transcutaneous delivery of vaccines, exploiting the accessibility and proven immune competence of the skin for enhanced immunity. The delivery of vaccines to the skin, a tissue densely populated with antigen presenting cells and inherently adapted to respond to invading pathogens, has been shown in many contexts to improve the potency of immunity

multi-week periods, with persistent antigenic and inflammatory signals eliciting stronger responses than transient bolus vaccine exposure.<sup>[4,5]</sup> These findings are consistent with known differences in the natural immunity generated against transient versus persistent pathogens, indicating specific mechanisms of immunity that may be exploited through engineered kinetics to yield greater vaccine efficacy.

We have recently begun to explore the combination of these two approaches for enhancing immunogenicity, through the

P. C. DeMuth,<sup>[+]</sup> Prof. D. J. Irvine  
Department of Biological Engineering  
Massachusetts Institute of Technology, (MIT)  
Cambridge, MA 02139 USA  
E-mail: djirvine@mit.edu  
Y. Min,<sup>[+]</sup><sup>[++]</sup> Prof. P. T. Hammond  
Department of Chemical Engineering  
MIT, Cambridge, MA, USA  
E-mail: hammond@mit.edu  
Prof. D. J. Irvine, Prof. P. T. Hammond  
Koch Institute for Integrative Cancer Research  
MIT, Cambridge, MA, USA

Prof. D. J. Irvine, Prof. P. T. Hammond  
Institute for Soldier Nanotechnologies  
MIT, Cambridge, MA 02139 USA  
Prof. D. J. Irvine  
Department of Materials Science and Engineering  
MIT, Cambridge, MA 02139 USA  
Prof. D. J. Irvine  
Ragon Institute of MGH, MIT, and Harvard  
Charlestown, MA 02129 USA  
Prof. D. J. Irvine  
Howard Hughes Medical Institute  
Chevy Chase, MD 20815 USA

<sup>[+]</sup>P.C.D. and Y.M. contributed equally to this work.

<sup>[++]</sup>Present Address: Department of Polymer Engineering, University of Akron, Akron, OH, USA



DOI: 10.1002/adhm.201300139

design and testing of microneedle platforms capable of controlling the kinetics of vaccine delivery in vivo. Microneedle patches composed of a single monolithic polymer phase require that patches remain on the skin for prolonged time periods to achieve extended drug release. Conversely, our previous composite microneedle structures, based on solid biodegradable poly(lactide-co-glycolide) (PLGA) polymer tips supported on a water-soluble poly(acrylic acid) (PAA) base rapidly disintegrate upon skin application, implanting the solid polymer tips into the skin following a brief  $\approx 5$  min application.<sup>[8]</sup> The implanted polymer tips can subsequently provide sustained release of encapsulated cargos over a tunable period of days to weeks. In these previous studies, vaccination utilizing PLGA/PAA composite microneedles implanting persistent polymer depots for slow cutaneous release of adjuvant following bolus antigen delivery yielded improved proliferation, stronger antigen-dependent cytokine secretion, and altered memory phenotypes in assays of CD8<sup>+</sup> T-cell immunity.<sup>[8]</sup> Here, we have expanded upon this concept through the design of a microneedle system based on silk protein, creating implantable hydrogel microneedle matrices for efficient vaccine loading and highly tailorable vaccine release kinetics in vivo. Unlike PLGA, loading of biomolecules in silk protein matrices is a simple one-step process. Silk has previously been used for high-density loading of sensitive biomolecules into non-immunogenic hydrogels under mild aqueous processing conditions, which subsequently release entrapped cargo for extended periods of time.<sup>[9,10]</sup> Recent work has demonstrated the ability of dried silk hydrogels to form dense microneedle structures that can be inserted into murine skin ex vivo.<sup>[11,12]</sup> The additional capacity for effective stabilization of vaccines and drugs in silk at room temperature offers an attractive opportunity to formulate vaccines that could avoid the cold chain, thus making vaccines more inexpensive and readily available.<sup>[13]</sup>

Here, we sought to combine the advantages of our implantable-tip composite microneedle design with the beneficial properties of silk as a controlled release matrix for entrapped proteins, and explored the ability of silk/PAA composite microneedles to regulate the kinetics of vaccine delivery in skin with the goal of mimicking patterns of antigen and inflammatory signal exposure during natural infections. Composite microneedles were loaded with an adjuvanted whole-protein subunit vaccine encapsulated in either PAA pedestals (providing a rapid initial bolus of vaccine release), or silk tips, which mediate slow/sustained vaccine release over time. We observed dramatic variations in the strength of antigen-specific T-cell responses dependent upon the temporal patterns of bolus and extended vaccine delivery programmed through materials engineering of the silk-composite structure. Combined with the recently demonstrated room temperature stability of vaccines embedded in silk,<sup>[13]</sup> this controlled-release microneedle platform has the potential to combine three important features of next-generation vaccines for use in the developing world: i) needle-free delivery, ii) inexpensive long-term room temperature storage without the need for a "cold chain," and iii) effective single-dose immunization providing potent immunological memory. Additionally, we have confirmed through these studies the potential for engineering optimal immune responses through programmed vaccine release kinetics, an important finding

supporting the future use of advanced drug delivery approaches in the progression of vaccine research.

## 2. Materials and Methods

### 2.1. Silk Fibroin Solution Preparation

Cocoons of *Bombyx mori* silkworm silk were purchased from Aurora Silk (Portland, OR). All other chemicals were purchased from Sigma-Aldrich (St. Louis, MO) and used as received. Silk fibroin was prepared from cocoons as previously described.<sup>[14]</sup> Briefly, cocoons were boiled for 40 min in a solution of 0.02 M sodium carbonate and then rinsed thoroughly with deionized water to extract the glue-like sericin protein. After drying, the extracted silk was dissolved in 9 M lithium bromide solution at 60 °C for 4 h, and subsequently the salt was removed by dialysis against deionized water using a Slide-a-Lyzer dialysis cassette (Pierce, Rockford, IL) for 48 h, changing the water regularly at least six times. The resulting solution was centrifuged twice ( $\approx 12\,700$  rcf) at 4 °C for 20 min to remove impurities and the aggregates that formed during dialysis. The supernatant was stored at 4 °C and filtered through a 450-nm syringe filter prior to use. The final concentration of silk fibroin solution was determined by weighing the residual solid of a known volume of solution after drying.

### 2.2. Fabrication of Silk/PAA Microneedle Arrays

Poly(dimethyl siloxane) (PDMS) microneedle molds (Sylgard 184, Dow-Corning, Midland, MI) were prepared using a Clark-MXR-CPA-2010 laser micromachining instrument (VaxDesign Inc., Orlando, FL). Soluble ovalbumin (OVA, Worthington, Lakewood, NJ) and polyI:C (Invivogen, San Diego, CA) were combined with aqueous silk solutions (8% w/v) to give the desired immunogen concentration (generally  $\approx 5$  mg mL<sup>-1</sup> OVA, 0.5 mg mL<sup>-1</sup> polyI:C). PDMS molds were then treated with O<sub>2</sub> plasma before addition of silk-vaccine formulations to the mold surface by pipette. Molds were centrifuged for 30 min at rcf  $\approx 450$  and excess silk-vaccine solution was removed from the mold surface for potential reuse. Molds containing silk-vaccine were then dried at 25 °C for 12 h and treated with 9:1 (v/v) methanol:water for 5 min or left untreated. Polyacrylic acid (PAA, 250 kDa, 35%) was added to soluble OVA and polyI:C at the desired concentrations (generally  $\approx 1$  mg mL<sup>-1</sup> OVA,  $\approx 0.1$  mg mL<sup>-1</sup> polyI:C) and mixed well. PAA pedestals were then formed through addition of 35% PAA to the mold surface, followed by centrifugation (30 min, rcf  $\approx 450$ ) and drying at 25 °C (48 h on the benchtop, followed by 2–14 d under desiccation), before removal. All microneedles were stored under desiccation at 25 °C for at least 2 months prior to use. Microneedle arrays were characterized by optical and confocal microscopy using a Leica DMXR and a Zeiss LSM 510 respectively. Total vaccine loading was determined using fluorescently labeled OVA as described below. PolyI:C loading was determined similarly following elution into phosphate buffered saline (PBS) using a ribogreen RNA detection kit (Invitrogen) to determine the loaded RNA concentration.

### 2.3. In Vitro Vaccine Release

Silk implant release was characterized in vitro through brief (<30s) exposure of fabricated arrays to deionized water. Implants were then collected through centrifugation and washed before application of aqueous suspensions to glass coverslips. After drying, implants were imaged by SEM using a JEOL 6700F FEG-SEM.

To differentiate the release kinetics of OVA loaded in PAA or silk and to evaluate the effect of methanol treatment on release profiles, in vitro OVA release experiments were performed by immersing silk/PAA composite microneedles in PBS buffer at pH 7.4 and  $37 \pm 0.5$  °C. Dried silk tips in PDMS were fabricated as described above with or without treatment in 9:1 (v/v) methanol:water solution for 5 min prior to PAA addition. Three experimental groups ( $n = 4$  for each group) were designed: AlexaFluor 555 labeled ovalbumin (AF555-OVA) loaded in PAA, AlexaFluor 647 labeled ovalbumin (AF647-OVA) loaded in non-treated silk tips, AF647-OVA loaded in methanol-treated silk tips. For AF555-OVA release from the PAA portion of composite microneedles, 1 mL aliquots were removed from a 10 mL volume release bath at predetermined time points and replaced with 1 mL of fresh pre-warmed PBS. For AF647-OVA release from the untreated or methanol-treated silk portion, microneedles were transferred between 0.5 mL aliquots of fresh prewarmed PBS at pre-set time points. The concentration of AF555-OVA and AF647-OVA in each of the release samples was quantified by fluorescence spectroscopy (M200 Pro, Tecan, Mannedorf, Switzerland). At each time point, samples were loaded in triplicate and the averaged reading was taken for further quantification.

### 2.4. In Vivo Microneedle Application and Vaccine Release

All animal studies were approved by the MIT IUCAC and animals were cared for in the USDA-inspected MIT Animal Facility under federal, state, local, and NIH guidelines for animal care. Microneedle application experiments were performed on anesthetized C57BL/6 mice (Jackson Laboratories, Bar Harbor, ME) at the flank or dorsal ear skin. Skin was rinsed briefly with PBS and dried before application of microneedle arrays by gentle pressure. Following application, mice were euthanized at subsequent time points and the application site was dissected. Treated skin and applied microneedle arrays were imaged by confocal microscopy to assess transcutaneous delivery of silk implants. In some cases, treated skin was excised and fixed in 3.7% formaldehyde for 18 h, then incubated in 30% sucrose/PBS for 2 h before embedding in optimal cutting temperature medium (OCT, Tissue-Tek) for histological sectioning on a cryotome. Histological sections were then imaged using confocal microscopy. Live whole animal imaging was performed using a Xenogen IVIS Spectrum (Caliper Life Sciences, Hopkinton, MA) on anesthetized mice. For luminescent imaging of myeloperoxidase (MPO)-dependent oxidative burst, luminol sodium salt (Santa Cruz Biotech, Santa Cruz, CA) was administered i.p. ( $250 \text{ mg kg}^{-1}$ ) before imaging. Fluorescence/luminescence data were processed using region of interest (ROI) analysis with background subtraction and internal control ROI comparison

to untreated skin using the Living Image 4.0 software package (Caliper).

### 2.5. Immunizations

C57Bl/6 mice (5/group) were immunized on day 0 with 9  $\mu\text{g}$  ovalbumin and 150 ng polyI:C by intradermal (i.d.) injection (15  $\mu\text{L}$  in the dorsal caudal ear skin) or by microneedle array (5 min application). Microneedles contained  $\approx 98\%$  of the total vaccine dose in the PAA fraction, with the remaining 2% in the silk implant. Silk implants were either left untreated or cross-linked with methanol as previously described to give differential vaccine release kinetics. In some cases, microneedles were fabricated to contain vaccine in only silk implants, or otherwise in only the PAA pedestal. Animals vaccinated by i.d. injection received an identical boost on day 28. Mice were then challenged on day 77 with 10  $\mu\text{g}$  pCl-neo-sOVA (pOVA, Addgene, Cambridge, MA) encoding soluble OVA, by intramuscular (i.m.) injection (25  $\mu\text{L}$ , split between both quadriceps).

### 2.6. In Vivo Murine Immunogenicity

Frequencies of OVA-specific CD8<sup>+</sup> T cells and their phenotypes elicited by immunization were determined by flow cytometry analysis of peripheral blood mononuclear cells (PBMCs) at selected time points following staining with DAPI (to discriminate live/dead cells), anti-CD8 $\alpha$ , anti-CD44, anti-CD62L, (BD Biosciences, San Jose, CA), and phycoerythrin-conjugated SIINFEKL/H-2K<sup>b</sup> peptide-MHC tetramers (Beckman Coulter, Indianapolis, IN). To assess the functionality of primed CD8<sup>+</sup> T cells, PBMCs were stimulated ex vivo with 10  $\mu\text{g mL}^{-1}$  OVA-peptide SIINFEKL for 6 h with Brefeldin-A (Invitrogen, San Diego, CA), fixed, permeabilized, stained with anti-IFN $\gamma$ , anti-TNF $\alpha$ , and anti-CD8 $\alpha$  (BD Biosciences), and analyzed by flow cytometry. Anti-ovalbumin or anti-silk IgG, IgG<sub>1</sub>, IgG<sub>2C</sub>, and IgM titers, defined as the dilution of sera at which 450 nm OD reading was 0.25, were determined by ELISA analysis of sera from immunized mice. To measure avidity index, ELISA was performed after 10 min exposure of bound serum to 6 M urea, to strip weakly bound immunoglobulins.<sup>[15]</sup> IgG avidity index was calculated as the ratio of measured titer without urea treatment to titer measured with urea treatment.

## 3. Results

### 3.1. Fabrication of Silk-PAA Composite Microneedles

We recently reported a strategy for the fabrication of composite microneedles based on PAA and PLGA for microneedle-mediated implantation of solid PLGA micro-tips or microspheres in skin.<sup>[8]</sup> Here, we adapted this approach to create microneedles bearing a solid silk tip supported by a PAA pedestal, intended to rapidly dissolve in cutaneous tissue fluids following needle insertion, releasing silk tips for retention in the skin following

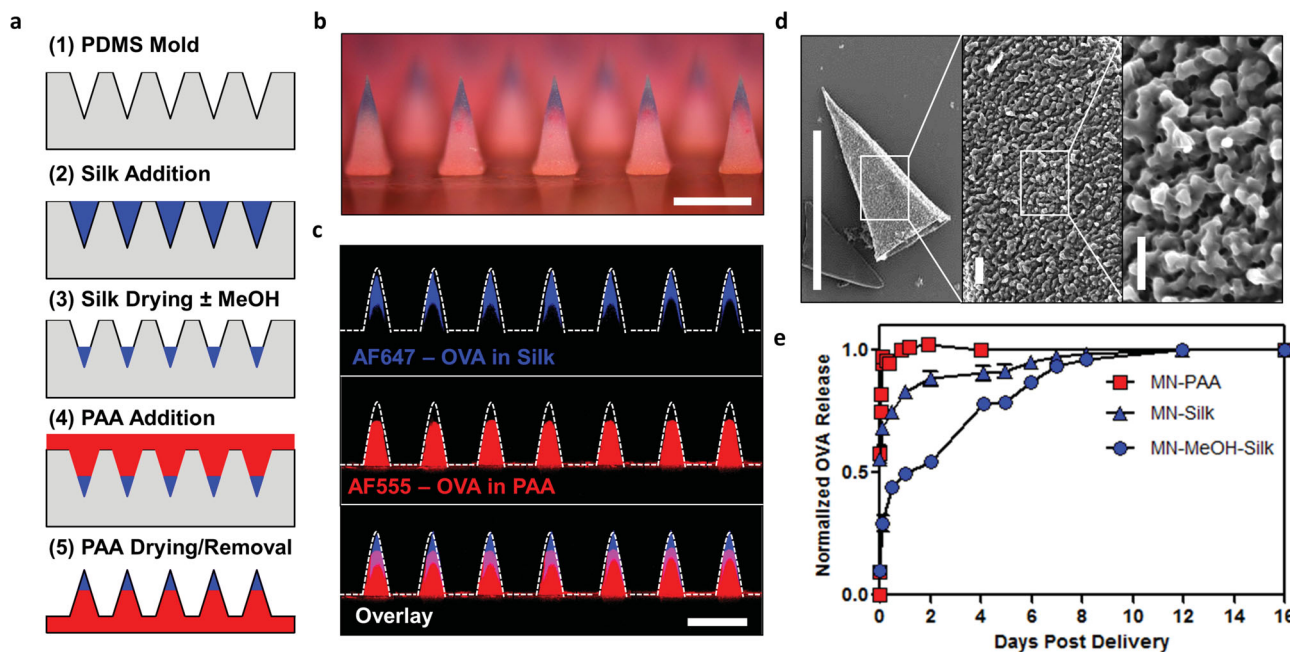


**Figure 1.** Fabrication and in vitro characterization of silk–PAA composite microneedles. a) Schematic of microneedle fabrication: (1) PDMS molds were fabricated using laser ablation, (2) silk–vaccine formulations were added to plasma-treated molds and infiltrated into mold cavities by centrifugation, (3) silk was dried in mold cavities forming hardened tips and left untreated or exposed to MeOH, (4) vaccine-loaded PAA was added to the mold and infiltrated into mold cavities by centrifugation, and (5) arrays were dried before removal. b) Optical image of silk/PAA microneedle array encapsulating AF647-OVA (blue) in silk tips, and AF555-OVA (red) in PAA pedestals (scale bar - 500  $\mu\text{m}$ ). c) Confocal images of composite microneedles showing AF647-OVA (blue) in silk tips and AF555-OVA (red) in PAA pedestals (scale bar - 500  $\mu\text{m}$ ). d) SEM images of a separated silk tip following 30 s exposure of a composite array to deionized water. Images show intact tip structure (left, scale bar - 500  $\mu\text{m}$ ) and micro-porous silk hydrogel structure (center, scale bar - 20  $\mu\text{m}$ , and right, scale bar - 5  $\mu\text{m}$ ). e) Quantitative analysis of fluorescent OVA release from silk and PAA fractions of composite microneedles over time.

microneedle patch removal. To fabricate these structures, we first generated PDMS molds bearing square pyramidal micro-scale cavities across their surface using laser ablation as previously described (Figure 1a, step 1).<sup>[16]</sup> We then surface-treated the molds with  $\text{O}_2$  plasma to generate a hydrophilic surface and facilitate infiltration of the mold cavities by the silk–vaccine solution. Silk fibroin protein was co-dissolved in aqueous solution with ovalbumin protein (OVA, a model antigen) and the TLR-3 agonist polyI:C, a potent double-stranded RNA adjuvant for stimulating antiviral immune responses.<sup>[17]</sup> This solution was added to plasma-treated molds and infiltration of the mold cavities was further completed through centrifugation (Figure 1a, step 2). After removing excess silk–vaccine solution, silk-filled molds were allowed to dry at room temperature for 12 h to produce hardened silk hydrogel tips within the PDMS molds (Figure 1a, step 3).<sup>[11,12]</sup> Silk protein is known to undergo increases in crystallinity due to the formation of beta sheets upon exposure to methanol, effectively producing physical crosslinks within silk matrices; this results in lowered diffusivity of drug, and prolonged cargo release from rehydrated silk hydrogels.<sup>[14]</sup> Here, we exposed solidified silk tips to methanol by pipetting solvent onto the mold surface, to enhance crystallite formation and retard release of encapsulated vaccine from silk tip implants following implantation in vivo (Figure 1a, step 3). Following methanol treatment, we added vaccine-loaded aqueous PAA solutions carrying co-dissolved OVA and polyI:C to the mold surface and again performed

centrifugation to compact the PAA into the mold cavities, forming complete PAA pedestal structures (Figure 1a, step 4). Microneedles were then dried in the mold at room temperature for several days and placed under vacuum to complete the drying process before removal and storage under vacuum at 25  $^\circ\text{C}$  (Figure 1a, step 5). This process reliably produced arrays of composite pyramidal microneedles 550  $\mu\text{m}$  in height and 250  $\mu\text{m}$  in width at the base ( $586 \pm 7 \mu\text{m}$  center to center distance,  $4.7 \pm 0.6 \mu\text{m}$  tip radius) bearing a tip–pedestal structure where vaccine-containing silk hydrogel tips were supported by vaccine-loaded PAA pedestals (Figure 1b). This structure was readily visible by optical microscopy imaging of microneedles fabricated with Alexafluor 647-labeled OVA (AF647-OVA) and Alexafluor 555-labeled OVA (AF555-OVA) loaded within the silk tip and PAA pedestal, respectively (Figure 1b). We further confirmed this needle microstructure using confocal microscopy to detect the localization of the vaccine cargo within the tip or pedestal of the resulting microneedles. This analysis revealed AF647-OVA restricted to the silk tip of each microneedle with AF555-OVA signal observed only in the PAA pedestal (Figure 1c). Given our previous results with similar PLGA/PAA systems, we expected that this composite structure would allow for effective cutaneous insertion of the hardened composite microneedles, where exposure to interstitial fluids would rapidly dissolve the PAA pedestals releasing the silk tips, which would remain implanted in the skin following removal of the array backing.<sup>[18]</sup>

### 3.2. In Vitro Characterization of Silk Tip Release and Vaccine Cargo Delivery

To test our expectation that composite silk–PAA microneedles would rapidly release silk tips upon exposure to tissue fluids in vivo, we exposed microneedle arrays to deionized water in vitro for short periods of time to observe PAA dissolution and silk tip release. Here, we visually observed rapid and complete separation of silk tips from PAA composite microneedle arrays after only 30 s of immersion. We then collected the separated silk tips by centrifugation and imaged them using SEM to observe their structure. Collected tips maintained their pyramidal geometry with dimensions consistent with the molds used in their fabrication (Figure 1d). Further, high magnification SEM imaging of released tips revealed a nano-porous network structure consistent with bundling of silk proteins to form a self-assembled network structure (Figure 1d).

To confirm the ability of composite silk–PAA microneedles to provide control over vaccine release profiles, we fabricated microneedle arrays containing AF647-OVA loaded in the silk needle tips or AF555-OVA in the PAA pedestals. Silk tips were either left untreated or treated with methanol as before to introduce additional cross-linking into the silk hydrogels. We then immersed each array in PBS pH 7.4 at 37 °C and collected fractions of the solution at subsequent time points to measure the release of encapsulated OVA protein by fluorescence spectroscopy. Consistent with expectations, AF555-OVA loaded into the PAA phase was rapidly dispensed from dissolving pedestals, with complete release over the course of only 2 h (Figure 1e). Conversely, AF555-OVA loaded into silk hydrogel tips was released more slowly with kinetics further modulated by methanol exposure during fabrication. For microneedles bearing untreated silk tips, AF647-OVA exhibited a burst release of  $\approx 70\%$  over the course of 2 h with sustained release of the remaining 30% over the next 5–6 d (Figure 1e). Delivery from methanol-treated silk was further delayed with only 25% burst release over 2 h, and sustained near zero-order release of the remaining 75% over the course of 8–12 days (Figure 1e). Thus, the combination of rapidly dissolving PAA with the slow swelling of silk hydrogels permits the kinetics of vaccine release to be varied over a wide range, spanning from tens of seconds to more than a week.

### 3.3. Composite Microneedles Rapidly Implant Silk Tips to Form Cutaneous Vaccine Depots In Vivo

We previously demonstrated that composite PLGA/PAA microneedles penetrate skin, and prior work has also shown the ability of solid silk microneedles to effectively insert into murine skin.<sup>[11]</sup> To confirm the ability of composite silk–PAA microneedles to effectively penetrate the skin, we fabricated microneedles encapsulating AF647-OVA and AF555-OVA in the silk and PAA microneedle phases, respectively, and applied these arrays to the skin of C57Bl/6 mice for 5 min. Confocal imaging of microneedle arrays before and after application revealed complete loss of both silk- and PAA-associated OVA fluorescent signal from the length of each microneedle following 5 min insertion in skin (Figure 2a). Confocal imaging on excised skin or skin histological sections where patches were applied revealed

overlaid punctate fluorescent signal from AF647-OVA and AF555-OVA at individual sites of microneedle insertion indicating the effective delivery of both silk- and PAA-loaded materials upon microneedle penetration into the cutaneous space (Figure 2b,c). In these images, microneedles were observed to insert several hundred microns below the skin surface in the epidermal space, consistent with previous demonstrations of microneedle delivery.<sup>[3,8,18]</sup> Three-dimensional rendering of confocal z-stacks to visualize the depth of fluorescent OVA delivery showed fluorescent signals from AF647- and AF555-OVA from silk and PAA respectively, extending several hundred micrometers below the skin surface at sites of microneedle insertion (Supplementary Figure 1, Supporting Information). Further, similar to our previous results, we visually observed healing of the microscopic skin defects created during microneedle application within 1 d of treatment.<sup>[8]</sup> Together these results confirm the ability of silk–PAA microneedles to effectively insert into murine skin, with rapid dissolution of the PAA pedestal upon exposure to skin fluids to leave behind vaccine-loaded silk hydrogels.

To simplify the fabrication scheme in these proof-of-concept studies, active agent was contained within the entire PAA fraction of the composite microneedle array, including the patch backing as well as the individual needle pedestals. Thus, although Figure 2a shows that active agent from the needle pedestals is completely lost during application, an effective efficiency of delivery accounting for the entire PAA phase including the patch backing was calculated to be 3%. This low overall efficiency of delivery could be corrected through a multi-step PAA addition during fabrication to generate patches with active agent loaded only into the needle pedestals, thus eliminating wasted material contained in the patch backing. However, for these proof-of-concept studies meant to explore the fundamental impact of prolonged delivery from implanted hydrogels, we chose to employ the simpler single-step fabrication approach. Importantly, all reported vaccine dosages below account for the amount of vaccine actually delivered into the skin from the PAA phase.

### 3.4. Cutaneous Silk Implants Control Vaccine Release Kinetics In Vivo

We next tested whether microneedle-delivered vaccine release in vivo could be programmed during array fabrication. Similar to previous experiments, we fabricated microneedles containing AF647-OVA and AF555-OVA in the silk or PAA needle fraction respectively, and applied these to the auricular skin of anesthetized C57Bl/6 mice. For comparison to parenteral administration, we performed i.d. injection of dose-matched soluble fluorescent vaccine formulations in the dorsal ear skin. We then used whole-animal fluorescence imaging to monitor the persistence of the OVA fluorescent signal at the treatment site and determine the release characteristics of injected or microneedle-delivered vaccine in vivo. Fluorescence imaging revealed the rapid loss of AF555-OVA signal in all test groups, indicating the clearance of soluble OVA from the treatment site within 24 h of delivery either by i.d. injection, or from the PAA phase of composite microneedles (Figure 2d,e). Clearance of AF647-OVA was similarly rapid in the case of i.d. injection. Conversely, AF647-OVA encapsulated in silk-implants was retained at the

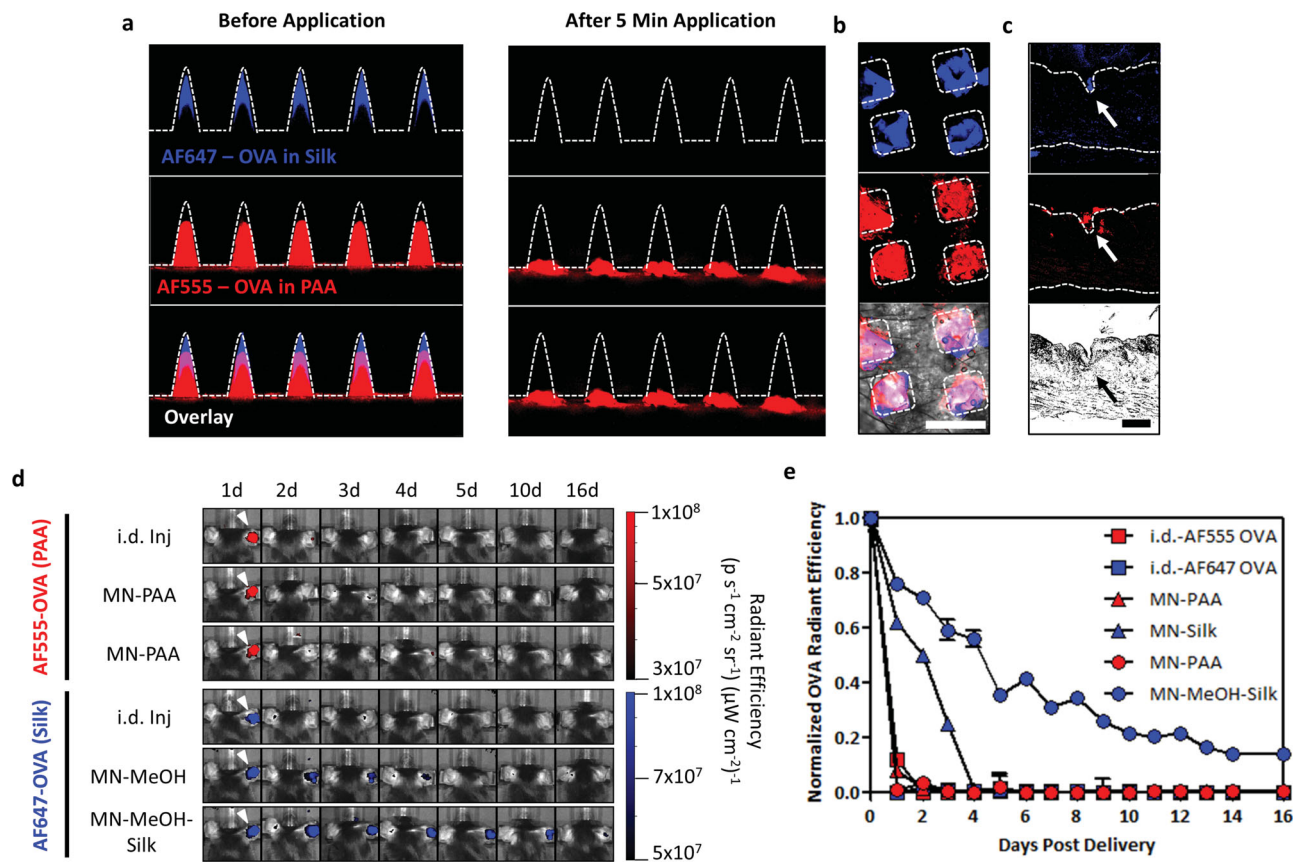


**Figure 2.** Composite microneedles deliver loaded vaccines to murine skin in vivo. a) Confocal micrographs of composite microneedles showing AF647-OVA (blue) in silk tips and AF555-OVA (red) in PAA pedestals (scale bar - 500  $\mu\text{m}$ ) before application (left) and following a 5 min application to murine auricular skin (right). b) Confocal micrographs showing OVA delivery to murine skin following 5 min application of composite microneedles (AF647-OVA in silk tips–blue, and AF555-OVA in PAA pedestals–red, insertion sites outlined, scale bar - 500  $\mu\text{m}$ ). c) Confocal micrograph of histologically sectioned skin treated for 5 min with composite microneedles (AF647-OVA in silk tips–blue, and AF555-OVA in PAA pedestals–red, scale bar - 100  $\mu\text{m}$ ). d) Whole animal fluorescent images of mice treated (arrows, right ear) with composite microneedles containing AF647-OVA (blue) in silk tips ( $\pm$ MeOH treatment) and AF555-OVA (red) in PAA pedestals. e) Quantitative analysis of total fluorescent OVA signal measured at the treatment site for mice receiving i.d. injection or microneedle delivery of AF647-OVA in silk tips ( $\pm$ MeOH treatment) and AF555-OVA in PAA pedestals.

treatment site for days to weeks following microneedle treatment, depending on whether methanol treatment was performed during fabrication to induce additional silk hydrogel beta sheet formation (Figure 2d,e). Animals treated with silk-PAA microneedles without methanol treatment showed nearly linear clearance of silk-loaded AF647-OVA over the course of 4 d following treatment. In the case of microneedles pretreated with methanol, AF647-OVA fluorescent signal was detectable at the treatment site for >16 d following array application (Figure 2d,e). Notably, distinct from the in vitro release pattern, these in vivo antigen release profiles showed no burst release. These results indicate the ability of microneedle-delivered silk tip implants to control the rate of vaccine release in vivo with a kinetic profile dependent on methanol treatment during fabrication.

### 3.5. Microneedle Vaccine Release Kinetics Determine the Strength of Cellular Immunity

Many natural infections are characterized by an initially abundant microbe burden lasting a few days, which is predominantly

eliminated by the initial immune response. However, in many “acute” infections, this initial elimination of microbes is followed by a delayed clearance of residual low levels of the pathogen that persist for a more prolonged period prior to complete eradication.<sup>[19–23]</sup> Thus the natural immune system is frequently exposed to a large pathogenic bolus of antigenic and inflammatory stimuli, followed by a prolonged low-level exposure, which can persist for days to months following acute infection. Given that such kinetic patterns in natural infection are often associated with profound T-cell responses and robust immune memory, we sought to determine whether tailoring vaccine exposure kinetics using silk-PAA microneedles to mimic this natural progression of infection would impact vaccine immunogenicity relative to bolus injection or bolus microneedle delivery. To mimic the adjuvant/inflammation kinetics described above for acute infection, microneedles were fabricated with the vaccine dose split (98% and 2%) between the PAA and silk fractions with or without methanol pretreatment (MN PAA(98)/Silk(2) and MN PAA(98)/MeOH-Silk(2)). The single-step fabrication approach for the silk tips used here, where the microneedle cavities are filled with silk/vaccine solution and

simply dried to form the silk tips, limited the capacity of the silk matrix to a theoretical maximum of only  $\approx 2\text{--}4\ \mu\text{g}$  of antigen loaded in the silk tips (total per patch). Since we could not generate PAA(0)/silk(100) arrays that would match the total vaccine dose of the PAA(98)/silk(2) microneedles and keep the fabrication process identical, we instead employed two alternative controls: microneedles were fabricated with either 98% of the vaccine dose in the PAA fraction (MN PAA(98)/Silk(0)) or 2% of the dose in the silk fraction (MN PAA(0)/Silk(2)), testing whether either of the vaccine partitions of the main test cases could replicate the response of the combined bolus±sustained release microneedles. The skin patches were further stored at

room temperature under desiccation for at least two months prior to use, to establish their ability to eliminate cold storage requirements for the vaccine.

We then vaccinated mice with  $9\ \mu\text{g}$  OVA and  $150\ \text{ng}$  polyI:C either by i.d. injection at the dorsal ear site (i.d. Inj.) or by microneedle administration as before. To monitor cellular immunity, we measured OVA-specific  $\text{CD8}^+$  T-cell proliferation in peripheral blood using SIINFEKL/H-2K<sup>b</sup> peptide-MHC tetramers (SIINFEKL is the immunodominant peptide epitope of OVA). This analysis revealed that i.d.-injected vaccines elicited extremely weak antigen-specific  $\text{CD8}^+$  T-cell responses, with minimal expansion of OVA-specific cells

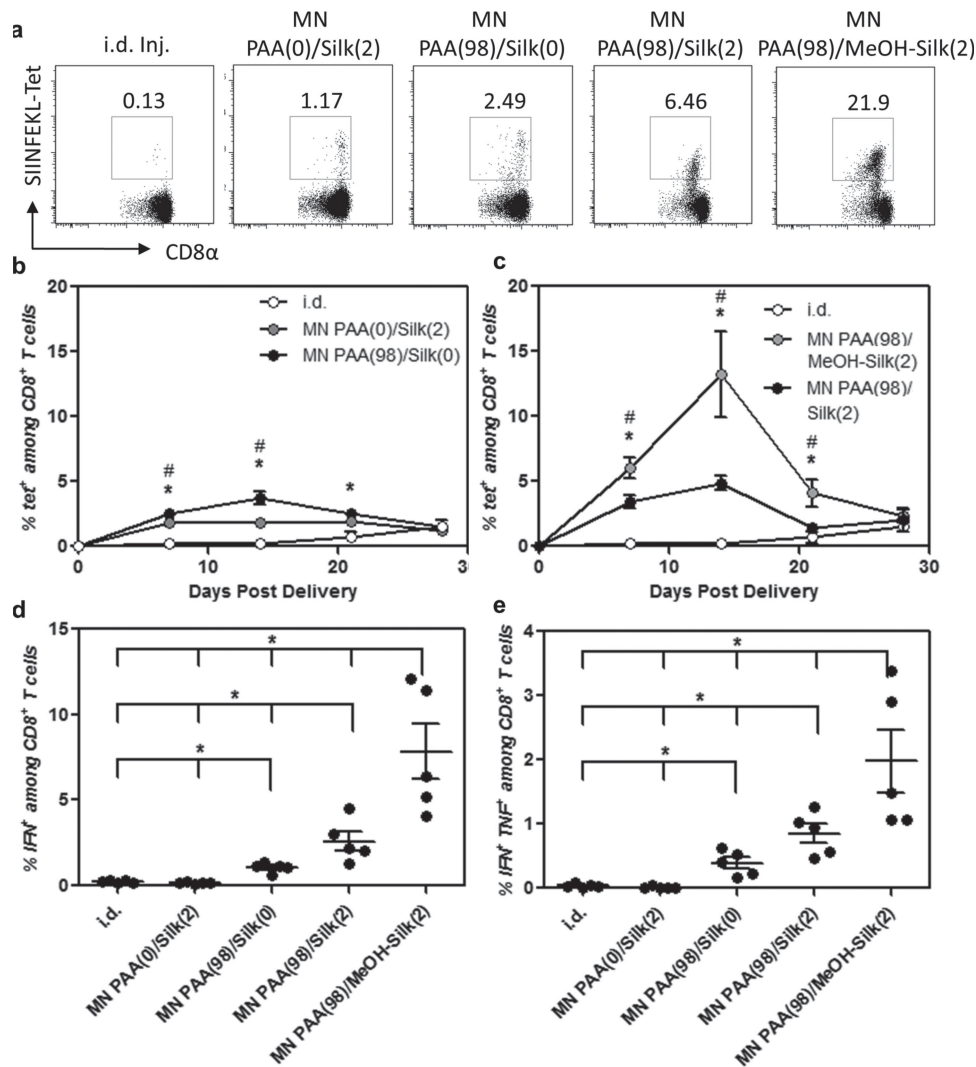


**Figure 3.** Prolonged vaccine release profile elicits increased proliferation of antigen-specific  $\text{CD8}^+$  T cells. C57Bl/6 mice ( $n = 5/\text{group}$ ) were vaccinated on day 0 either by i.d. injection or microneedle treatment ( $\pm\text{MeOH}$  to increase crystallinity of silk implants) with  $9\ \mu\text{g}$  OVA and  $150\ \text{ng}$  polyI:C. Microneedles were fabricated with 98% of the total vaccine dose in the PAA fraction, with the remaining 2% in the silk implant (MN PAA(98)/Silk(2) and MN PAA(98)/MeOH-Silk(2)); control microneedles were fabricated with either 98% of the total vaccine dose in the PAA (MN PAA(98)/Silk(0)) or 2% of the total dose in the silk fraction (MN PAA(0)/Silk(2)). a–c) Flow cytometry analysis of antigen-specific  $\text{CD8}^+$  T-cell proliferation in peripheral blood. Shown are a) representative cytometry plots from day 14, and b,c) quantitative analysis of SIINFEKL-tetramer<sup>+</sup>  $\text{CD8}^+$  T-cell frequencies for 4 weeks following vaccination. (b,  $*p < 0.05$  for MN PAA(98)/Silk(0) versus MN PAA(0)/Silk(2),  $\#p < 0.05$  for MN PAA(98)/Silk(0) and MN PAA(0)/Silk(2) versus i.d., c,  $*p < 0.05$  for MN PAA(98)/MeOH-Silk(2) versus MN PAA(98)/MeOH-Silk(2),  $\#p < 0.05$  for MN PAA(98)/MeOH-Silk(2) and MN PAA(98)/Silk(2) versus i.d.). d–e) Flow cytometry analysis of inflammatory cytokine expression following ex vivo antigen restimulation following ex vivo antigen restimulation. Shown is quantitative analysis of  $\text{IFN}\gamma^+$  and  $\text{IFN}\gamma^+/\text{TNF}\alpha^+$   $\text{CD8}^+$  T cells measured on day 14. ( $*p < 0.05$ )

over 4 weeks following a single immunization ( $\approx 1\%$  of  $CD8^+$  T cells, **Figure 3a,b**). Microneedles carrying a fraction of the vaccine dose solely in the PAA or solely in the silk phase induced stronger  $CD8^+$  T-cell proliferation, reaching a few percent tetramer $^+$   $CD8^+$  T cells by 14 d following immunization (**Figure 3a,b**). Interestingly, for the two microneedle groups containing a small fraction of the vaccine dose in the silk tips and the bulk of the vaccine in the PAA phase, the T-cell response was stronger than each of the prior groups (**Figure 3a–c**). Strikingly, methanol-treated silk tip implants that provided a sustained low dose of the vaccine over 2 weeks after the initial bolus PAA release resulted in dramatic increases in the frequency of tet $^+$   $CD8^+$  T cells compared with the other vaccination regimens (**Figure 3a–c**). Two weeks following microneedle patch application, SIINFEKL-specific  $CD8^+$  T cells expanded to 10%–20% of all  $CD8^+$  T cells in this group. To test the functionality of these expanded T cells, we restimulated PBMCs on day 14 *ex vivo* with SIINFEKL and assessed production of the inflammatory cytokines IFN- $\gamma$  and TNF- $\alpha$  using intracellular staining. Flow cytometric analysis revealed high frequencies of antigen-specific functional cytokine-secreting  $CD8^+$  T cells in the case of microneedle vaccination, while i.d.-injected animals showed only background levels of activation, as expected from the tetramer-staining analysis (**Figure 3d,e**, and Supplementary Figure 2, Supporting Information). Sustained low-level vaccine exposure from methanol cross-linked silk tip implants resulted in significantly higher frequencies of IFN- $\gamma^+$  and IFN- $\gamma^+$  TNF- $\alpha^+$  multi-functional T cells compared with the other vaccine groups (**Figure 3d,e**, and Supplementary Figure 2, Supporting Information). Notably, the single silk/PAA composite microneedle treatment was able to induce  $CD8^+$  T-cell responses of similar magnitude and cytokine secretion capacity as those observed after a prime + boost regimen administered by i.d. injection (Supplementary Figure 3, Supporting Information). These significant increases in the magnitude of cellular immune responses suggest that both microneedle delivery and prolonged antigen/adjuvant delivery kinetics can substantially enhance the strength of the adaptive cellular immune response in transcutaneous vaccination.

Sustained antigen stimulus has been implicated in controlling memory cell phenotype and function.<sup>[6,7]</sup> Thus, we next compared the memory phenotype of  $CD8^+$  T cells elicited by single silk–PAA microneedle treatment to prime-boost vaccination administered by i.d. injection. We observed a significant increase in the frequency of  $CD44^+$   $CD62L^+$  central memory  $CD8^+$  T cells on day 63 following microneedle vaccination compared with injection (**Figure 4a,b**). Central memory T cells have previously been correlated with effective immunological responses through more rapid recall upon re-exposure to pathogen, and are thought to be important for long-term protection.<sup>[24]</sup> Finally, we measured the strength of  $CD8^+$  T-cell expansion upon recall *in vivo* with injected OVA-expressing plasmid DNA (pOVA). Here, we observed statistically identical expansion of SIINKEFL reactive, cytokine-secreting  $CD8^+$  T cells 14 d following recall challenge with pOVA in mice vaccinated once with silk–PAA microneedles or given two i.d. injections, suggesting that a single immunization by silk–PAA microneedle delivery can provide equivalent T-cell memory to a prime + boost parenteral vaccine (**Figure 4c–e**).

### 3.6. Microneedle Vaccination Gives More Potent and Balanced Humoral Immunity

To evaluate the antibody response elicited by composite silk–PAA microneedles vaccines, we collected sera from immunized mice on day 21 following a single i.d. injection of vaccine, MN PAA(98)/Silk(2) vaccination, MN PAA(98)/MeOH-Silk(2), or MN PAA(98)/Silk(0) vaccination. ELISA measurements of serum titers of OVA-specific IgM, IgG, IgG $_1$ , and IgG $_{2C}$  showed a consistent increase in the serum titers of class-switched OVA-specific antibodies for microneedle-immunized animals. Microneedle vaccines induced significant increases in serum titers for anti-OVA IgG, IgG $_1$ , and IgG $_{2C}$ , while no difference was observed for IgM (**Figure 5a–d**). The effect on “Th1-like” IgG $_{2C}$  antibody responses was particularly striking, as i.d. injection elicited no OVA-specific IgG $_{2C}$  response, while all microneedle groups elicited readily detectable IgG $_{2C}$  titers. These results suggest that microneedle delivery was able to elicit a more potent, Th1/Th2-balanced antibody repertoire compared with i.d. injection. However, sustained release of antigen from the silk tips was not required for this strong enhancement of humoral responses, as microneedles carrying vaccine only in the PAA phase elicited similarly high anti-OVA titers. We also analyzed the avidity of the elicited IgG responses using urea exposure before ELISA detection to strip away weakly binding immunoglobulins.<sup>[15]</sup> This analysis demonstrated significantly improved IgG avidity for mice receiving microneedle vaccines as compared with i.d. injected vaccines, with non-methanol-treated silk microneedles eliciting the greatest increase in avidity (**Figure 5e**). To confirm the low immunogenicity of silk protein used in these studies, we also measured the presence of silk-specific serum IgG by ELISA. In mice given i.d. injection or microneedle vaccines, no anti-silk IgG above the background of naïve mice was detected (Supplementary Figure 4, Supporting Information). Together, these results indicate that microneedle vaccines strongly augment the humoral response relative to traditional syringe injections, whether the vaccine is released in a bolus or over days to weeks.

### 3.7. Cutaneous Silk Implants Give Sustained Local Inflammatory Activation *In Vivo*

Finally, having shown the ability of composite silk–PAA microneedles to achieve prolonged vaccine release, we sought to determine whether persistent local inflammation in the case of MN PAA(98)/MeOH-Silk(2) immunizations might be contributing to the enhanced cellular immunity observed for these microneedle formulations. To this end, we used whole-animal luminescent imaging with the chemiluminescent probe luminol to longitudinally measure MPO-dependent oxidative flux in locally recruited inflammatory cells as an indication of inflammatory activation at the treatment site.<sup>[25,26]</sup> This approach has previously been used to observe recruitment of activated immune cells such as neutrophils and serves as a general marker for local innate inflammatory responses. Groups of mice were immunized by i.d. injection of OVA mixed with polyI:C as before, or treated with microneedles loaded with OVA and polyI:C in both the silk ( $\pm$ MeOH) and PAA fractions.

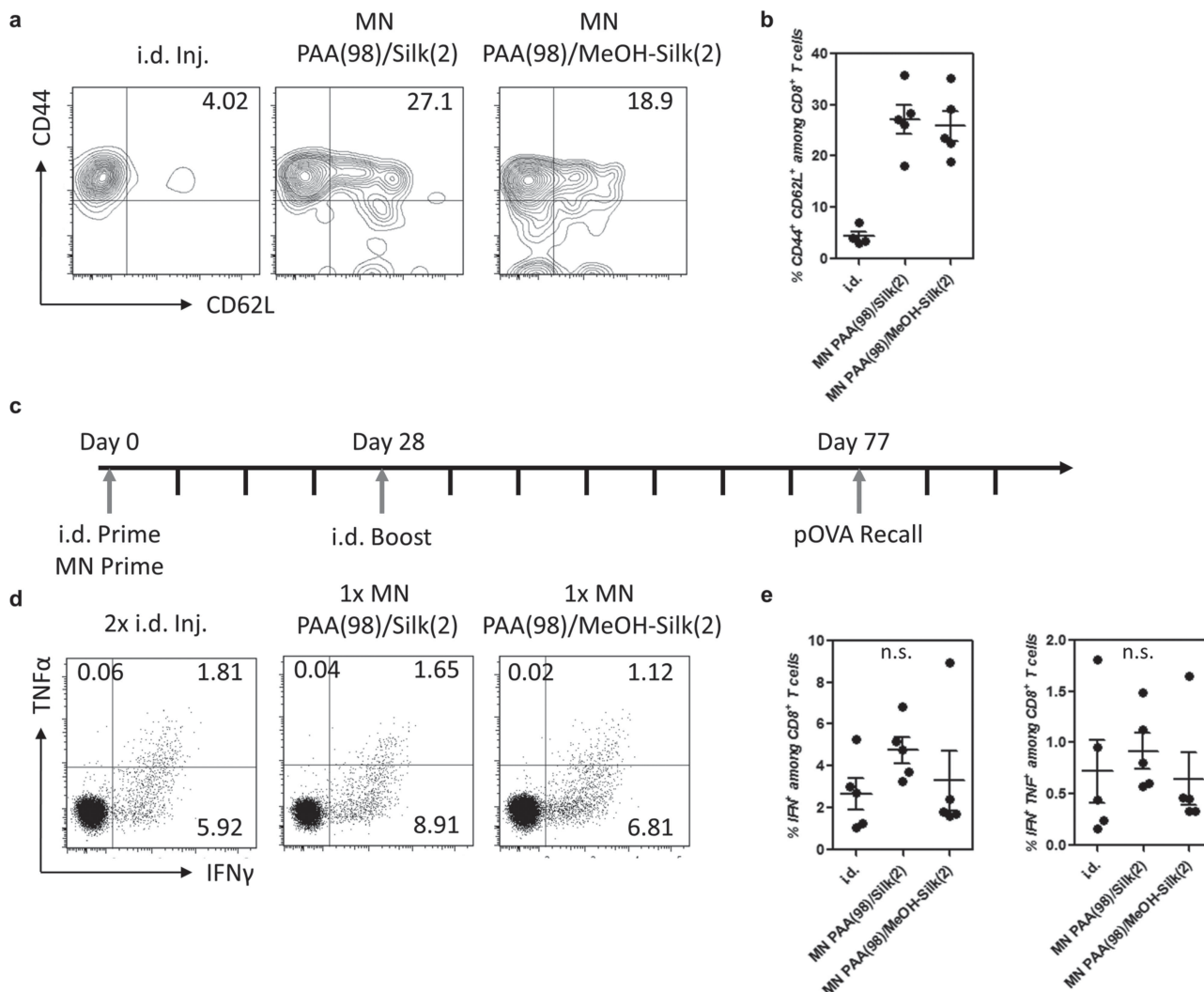


**Figure 4.** Microneedle vaccination gives enhanced memory CD8<sup>+</sup> T-cell phenotypes compared with traditional injections. C57Bl/6 mice ( $n = 5$ /group) were vaccinated on day 0 either by i.d. injection or microneedle treatment ( $\pm$ MeOH to cross-link silk implants) with 9  $\mu$ g OVA and 150 ng polyI:C. Microneedles were fabricated with 98% of the total vaccine dose in the PAA fraction, with the remaining 2% in the silk implant (MN PAA(98)/Silk(2) and MN PAA(98)/MeOH-Silk(2)); control microneedles were fabricated with either 98% of the total vaccine dose in the PAA (MN PAA(98)/Silk(0)) or 2% of the total dose in the silk fraction (MN PAA(0)/Silk(2)). a,b) Flow cytometry analysis of antigen-specific CD8<sup>+</sup> T-cell memory phenotype in peripheral blood. Shown are a) representative cytometry and b) quantitative analysis of CD44 and CD62L on SIINFEKL-tetramer<sup>+</sup> CD8<sup>+</sup> T cells on day 63 following vaccination. c–e) Immunized mice were recalled (timeline, (c)) by i.m. injection of 20  $\mu$ g pOVA on day 77. Shown are d) representative cytometry plots and e) quantitative analysis of IFN $\gamma$ <sup>+</sup> and IFN $\gamma$ <sup>+</sup>/TNF $\alpha$ <sup>+</sup> CD8<sup>+</sup> T cells measured on day 91 following ex vivo antigen restimulation of PBMCs (day 14 post recall).

Luminescent imaging indicated that i.d. injection produced only low-level inflammation at the treatment site, which resolved completely after 4 d (Figure 6a,b). Conversely, microneedle delivery with either untreated or methanol-treated silk/PAA microneedles showed a significant burst of inflammation for 3 d following treatment. After 5 d, mice vaccinated with untreated silk showed only background levels of MPO-dependent chemiluminescence, while methanol-treated silk microneedles gave significant luminescent signal above background on days 4, 5, and 11, suggesting persistent low-level inflammatory activation in these mice, likely resulting from prolonged release of antigen/adjuvant from the MeOH-treated silk implants. However, no visible signs of excessive inflammation or tissue

damage were observed in any of the mice in these treatment groups. Further, i.d. injection of 5x excess silk doses alone without adjuvant produced signal similar to i.d. injection alone, confirming the non-inflammatory nature of purified silk proteins in vivo (data not shown, reviewed elsewhere).<sup>[9]</sup> Finally, we have previously observed that sustained local delivery of polyI:C in the skin producing similar levels of luminol-dependent bioluminescent signal does not lead to measurable production of systemic cytokines, further suggesting the safety of this approach.<sup>[18]</sup> Together with the previous in vivo OVA delivery results, this indicates the ability of silk–PAA microneedles to sustain both antigen exposure and inflammatory cues from days to weeks following treatment in vivo. This sustained

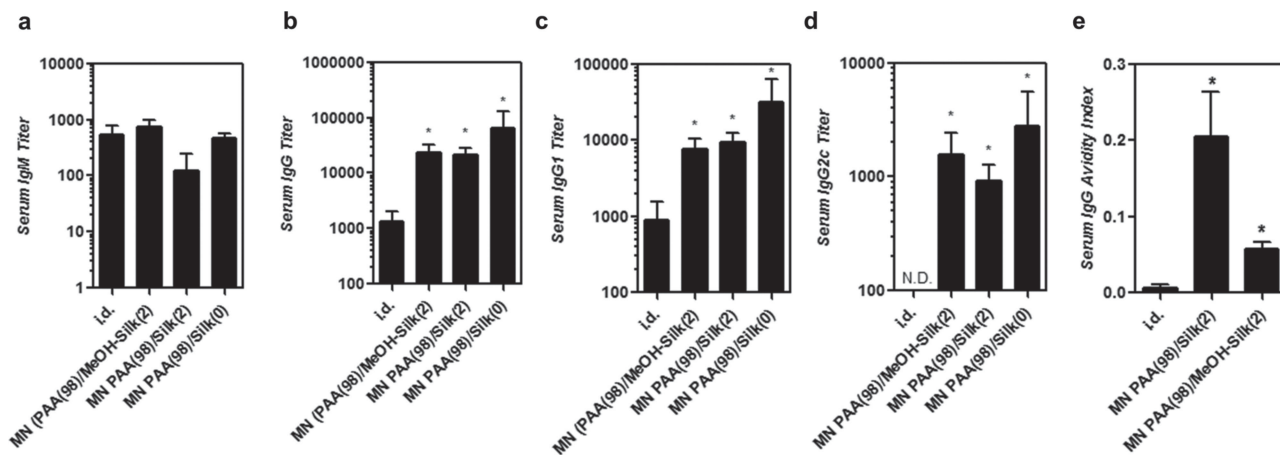


**Figure 5.** Delivery method determines the strength and isotype balance of humoral responses following i.d. or microneedle vaccination. C57Bl/6 mice ( $n = 5/\text{group}$ ) were immunized as in Figure 4. Shown are serum OVA-specific antibody titers and avidity indices measured on day 21. Serum OVA-specific antibody titers are shown for a) IgM, b) IgG, c) IgG<sub>1</sub>, and d) IgG<sub>2c</sub>. e) Avidity index for serum IgG, calculated as the ratio of titer measured without urea pretreatment of bound serum to titer with urea pretreatment. (\* $p < 0.05$  compared with i.d.).

low level of inflammation combined with continuous antigen delivery is likely a key factor in priming the potent CD8<sup>+</sup> T-cell proliferation observed following microneedle vaccination with methanol cross-linked silk tips.

#### 4. Discussion

The development of novel microneedle structures has yielded impressive progress in the advancement of effective, safe, and convenient delivery of macromolecules for vaccination in the skin.<sup>[18,27,28]</sup> These efforts have sought to effectively balance the many critical features essential for the effective clinical deployment of microneedle patch delivery systems including i) suitable mechanical properties, ii) control over micrometer-scale needle geometry and dimensions, iii) the ability to achieve rapid administration, iv) effective encapsulation of sensitive biomolecules, and v) avoidance of unwanted toxicity (reviewed elsewhere).<sup>[1]</sup> Here, we have demonstrated the fabrication and application of silk–PAA composite microneedle arrays that are well suited to address each of these design goals. These structured skin patches can encapsulate fragile protein or nucleic acid vaccine components in the silk phase, which has previously been demonstrated to protect vaccines in a dried state; and the microneedles readily penetrated murine skin, providing rapid deposition of vaccine into the skin over several minutes. Further composite silk–PAA microneedles provide robust flexibility in programming vaccine dosage and long-term delivery kinetics while retaining the ability to provide rapid and simple administration, a feature which we have shown to be critical for tuning the potency of immunity.

Previous studies of silk have shown effective loading of sensitive biomolecules including vaccines into silk matrices for storage at room temperature.<sup>[9,13,14,29]</sup> This is an attractive feature that could allow for inexpensive and broader global dissemination of vaccines to remote areas of the world. Here, we confirmed the potential for silk to stabilize subunit vaccines during room temperature storage, as all silk–PAA

microneedles used in these studies were stored at room temperature for >2 months prior to use. As observed previously, vaccine components entrapped within the dried PAA matrix are also protected during room temperature storage without loss of *in vivo* immunogenicity.<sup>[8]</sup> Prior studies of silk microneedles have demonstrated effective methods for fabrication as well as consistent insertion into murine skin.<sup>[11,12]</sup> We have expanded upon these results here to demonstrate a new approach for silk microneedle fabrication, taking advantage of the controlled release capacity for silk hydrogels while also improving the practicality of microneedle application via the releasable tip design. Recently, a similar approach for controlling vaccine release from microneedles has been described for the dermal implantation of chitosan reservoirs from poly(lactide) pedestals.<sup>[30]</sup> These embeddable chitosan microneedles showed control over week-long protein release resulting in enhanced humoral immune responses, indicating the potential of this approach for tuning immunity. Here, we have exploited the tunability of silk matrices for regulating vaccine release over days to weeks to demonstrate the impact of controlling vaccine kinetics on both cellular and humoral immunity.

It is well established that microneedle delivery of vaccines to the skin can enhance immunity through targeted delivery of antigen and adjuvant to response-governing antigen presenting cells present at high density within the skin. The physical disruption of the epidermal/dermal tissues during microneedle delivery is thought to be an important factor in mediating this enhanced immunity through the recruitment and maturation of antigen presenting cells.<sup>[2,3]</sup> Further, vaccine delivery in the context of epidermal wounding resulting from microneedle treatment may contribute to a pro-inflammatory microenvironment during cutaneous vaccination as keratinocytes and other skin-resident cells are known to actively sense and respond to tissue damage as well as pathogen-associate molecular patterns such as TLR-agonists.<sup>[31]</sup> Thus the success of microneedle delivery is likely in part founded in the natural mechanisms of the skin as a barrier to entry for sensing and responding to natural infections.

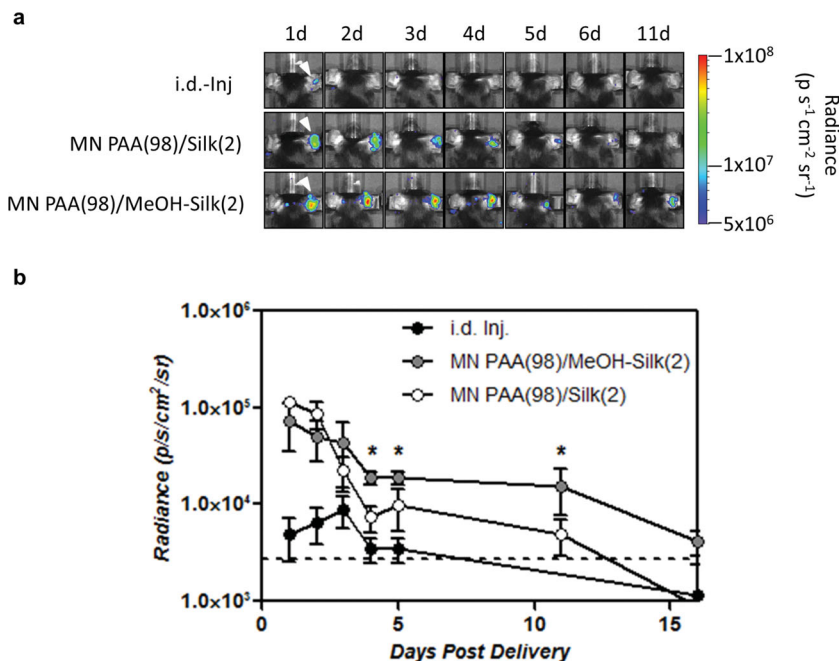


**Figure 6.** Vaccine-releasing composite microneedles prolong local inflammation. a) Whole animal chemiluminescent images of mice treated (arrows, right ear) with composite microneedles containing OVA and polyI:C in silk tips ( $\pm$ MeOH treatment) and PAA pedestals. Mice were imaged following luminal administration to visualize MPO-dependent oxidative flux in activated immune cells. b) Quantitative analysis of total luminescent signal measured at the treatment site for mice receiving i.d. injection or microneedle delivery of OVA and polyI:C in silk tips ( $\pm$ MeOH treatment) and PAA pedestals. ( $*p < 0.05$  compared to baseline.)

Here, we have shown that microneedle vaccination can be further enhanced through the adoption of a similar approach for replicating the natural time course of many diseases in which acute infection provides initially high levels of antigen and adjuvant stimuli which then rapidly decrease through immunological mechanisms of pathogen clearance, leading to long-term low levels of persistent pathogenic stimulus.<sup>[19–23]</sup> In previous studies, the presence of protein antigen or pathogen-derived genetic material has been observed for weeks to months in the local site of infection and in draining lymph nodes persisting after the relatively rapid clearance of infectious agent over the course of several days.<sup>[19,20,32,33]</sup> This pattern of sustained antigen exposure following primary clearance of infection has suggested a potential role for continued antigen/adjuvant stimulation in the development of primary effector and memory T-cell responses, including effects on T-cell migration/homing,<sup>[21]</sup> establishment of T-cell memory phenotypes,<sup>[34]</sup> and maintenance of effective long-lived protective T-cell responses.<sup>[35]</sup> Conversely, in some cases, chronic antigen presentation can lead to dysfunctional memory T-cell responses including loss of effector or proliferative functions or poor long-term survival.<sup>[36]</sup> This dichotomous development of either enhanced or defective long-term protective response is thought to be determined in part by the relative magnitude of sustained antigen exposure with chronic high antigen load frequently leading to exhausted or anergic phenotypes, while low level exposure commonly results in maintenance of protective functions. Thus the ability to finely tune the level and

persistence of antigenic or inflammatory cues following microneedle vaccination is likely critical for eliciting the desired effect on immunogenicity.

The silk–PAA composite microneedle system we have developed allows for vaccine delivery that can be tuned to replicate these timing and dosage features of natural infection through the combination of bolus vaccine release from rapidly soluble PAA, and extended release from vaccine-loaded silk depots implanted in the skin upon microneedle application. In our studies, this ability to provide bolus vaccine exposure combined with additional multi-week low-level delivery was able to drastically improve the proliferative capacity of antigen-specific T cells, yielding increased levels of peripheral antigen-specific, functionally active effector CD8<sup>+</sup> T cells greatly exceeding those responses generated through injection. These results indicate the need for both bolus vaccine delivery and sustained release as individual bolus or sustained release vaccine components gave much weaker responses. Further, the ability to program the duration of extended release proved important, as multi-week exposure resulted in 2.8-fold increases in CD8<sup>+</sup> T-cell responses over shorter multi-day release profiles. Notably, we observed that CD8<sup>+</sup> T-cell responses to

injected vaccines were only able to match immunizations with a single application of a microneedle patch following multiple vaccine doses, suggesting that the combination of microneedle delivery with programmed vaccine release may eliminate the need for prime-boost vaccine regimens.

## 5. Conclusions

Microneedle vaccines have traditionally exploited the naturally endowed immune-functionality of the skin as a primary barrier to pathogen entry, however further improvements to skin vaccination can be realized through the design of delivery approaches, which similarly mimic the natural time course of pathogen invasion, recognition, and response. Here, we have demonstrated the potency of this approach by designing a microneedle delivery strategy capable of mimicking the extended kinetic profile for antigen and adjuvant exposure following natural infection. Composite silk–PAA microneedles were able to rapidly disintegrate after insertion into the skin releasing vaccine bolus from dissolving PAA pedestals while simultaneously forming persistent cutaneous silk implants to mediate the sustained low-level delivery of vaccine over time. The flexibility of this approach for high-density loading and controllable release of biologically sensitive vaccine components allowed for programmable vaccine delivery in the skin to generate potent cellular and humoral immunity superior to prime vaccination by hypodermic injection. Notably, these

responses were elicited following months of microneedle storage at room temperature and gave equivalent immunity to those following prime-boost injection regimens. This ability for potent immunity following a single immunization, combined with the potential for long-term room temperature storage, and safe needle-free administration make this strategy an attractive option for effective global vaccine distribution, and deployment.

## Supporting Information

Supporting Information is available from the Wiley Online Library or from the author.

## Acknowledgements

This work was supported in part by the Ragon Institute of MGH, MIT, and Harvard, the NIH (AI095109), and the Department of Defense (contracts W911NF-13-D-0001 and W911NF-07-D0004, T.O. 8). D.J.I. is an investigator of the Howard Hughes Medical Institute. The authors would like to thank the Koch Institute for Integrative Cancer Research Cancer Center Support Grant and the Swanson Biotechnology Center core facilities it supports to facilitate this work. P.T.H. acknowledges support as David H. Koch Chair. The authors wish to dedicate this paper to the memory of Officer Sean Collier, for his caring service to the MIT community and for his sacrifice.

Received: April 15, 2013  
Published online: July 12, 2013

- [1] Y.-C. Kim, J.-H. Park, M. R. Prausnitz, *Adv. Drug Delivery Rev.* **2012**, *64*, 1547.
- [2] M. del Pilar Martin, W. C. Weldon, V. G. Zarnitsyn, D. G. Koutsonanos, H. Akbari, I. Skountzou, J. Jacob, M. R. Prausnitz, R. W. Compans, *mBio* **2012**, *3*, e00012.
- [3] P. C. DeMuth, J. J. Moon, H. Suh, P. T. Hammond, D. J. Irvine, *ACS Nano* **2012**, *6*, 8041.
- [4] C. M. Jewell, L. S. C. Bustamante, D. J. Irvine, *Proc. Natl. Acad. Sci. U.S.A.* **2011**, *108*, 15745.
- [5] P. Johansen, T. Storni, L. Rettig, Z. Qiu, A. Der-Sarkissian, K. A. Smith, V. Manolova, K. S. Lang, G. Senti, B. Mullhaupt, T. Gerlach, R. F. Speck, A. Bot, T. M. Kundig, *Proc. Natl. Acad. Sci. U.S.A.* **2008**, *105*, 5189.
- [6] M. F. Bachmann, R. R. Beerli, P. Agnellini, P. Wolint, K. Schwarz, A. Oxenius, *Eur. J. Immunol.* **2006**, *36*, 842.
- [7] A. Shaulov, K. Murali-Krishna, *J. Immunol.* **2008**, *180*, 1131.
- [8] P. C. DeMuth, W. F. Garcia-Beltran, M. L. Ai-Ling, P. T. Hammond, D. J. Irvine, *Adv. Funct. Mater.* **2012**, *23*, 161.
- [9] E. M. Pritchard, D. L. Kaplan, *Expert Opin. Drug Delivery* **2011**, *8*, 797.
- [10] E. Wenk, H. P. Merkle, L. Meinel, *J. Controlled Release* **2011**, *150*, 128.
- [11] K. Tsiaris, W. K. Raja, E. M. Pritchard, B. Panilaitis, D. L. Kaplan, F. G. Omenetto, *Adv. Funct. Mater.* **2012**, *22*, 330.
- [12] X. You, J.-H. Chang, B.-K. Ju, J. J. Pak, *Mater. Sci. Eng., C* **2011**, *31*, 1632.
- [13] J. Zhang, E. Pritchard, X. Hu, T. Valentin, B. Panilaitis, F. G. Omenetto, D. L. Kaplan, *Proc. Natl. Acad. Sci. U.S.A.* **2012**, *109*, 11981.
- [14] D. N. Rockwood, R. C. Preda, T. Yucel, X.-Q. Wang, M. L. Lovett, D. L. Kaplan, *Nat. Protoc.* **2011**, *6*, 1612.
- [15] Y. Yue, W. Xu, L. Hu, Z. Jiang, S. Xiong, *Virology* **2009**, *386*, 438.
- [16] P. C. DeMuth, X. Su, R. E. Samuel, P. T. Hammond, D. J. Irvine, *Adv. Mater.* **2010**, *22*, 4851.
- [17] C. Stahl-Hennig, M. Eisenblaetter, E. Jasny, T. Rzehak, K. Tenner-Racz, C. Trumppfeller, A. M. Salazar, K. Ueberla, K. Nieto, J. Kleinschmidt, R. Schulte, L. Gissmann, M. Mueller, A. Sacher, P. Racz, R. M. Steinman, M. Uguccioni, R. Ignatius, *PLoS Pathogens* **2009**, *5*, e1000373.
- [18] P. C. DeMuth, Y. Min, B. Huang, J. A. Kramer, A. D. Miller, D. H. Barouch, P. T. Hammond, D. J. Irvine, *Nat. Mater.* **2013**, *12*, 367.
- [19] W.-H. W. Lin, R. D. Kouyos, R. J. Adams, B. T. Grenfell, D. E. Griffin, *Proc. Natl. Acad. Sci. U.S.A.* **2012**, *109*, 14989.
- [20] D. L. Turner, L. S. Cauley, K. M. Khanna, L. Lefrancois, *J. Virol.* **2007**, *81*, 2039.
- [21] D. J. Zammit, D. L. Turner, K. D. Klonowski, L. Lefrancois, L. S. Cauley, *Immunity* **2006**, *24*, 439.
- [22] T. S. Kim, M. M. Hufford, J. Sun, Y.-X. Fu, T. J. Braciale, *J. Exp. Med.* **2010**, *207*, 1161.
- [23] K. N. Reetoo, S. A. Osman, S. J. Illavia, C. L. Cameron-Wilson, J. E. Banatvala, P. Muir, *J. Gen. Virol.* **2000**, *81*, 2755.
- [24] F. Sallusto, J. Geginat, A. Lanzavecchia, *Annu. Rev. Immunol.* **2004**, *22*, 745.
- [25] S. Gross, S. T. Gammon, B. L. Moss, D. Rauch, J. Harding, J. W. Heinecke, L. Ratner, D. Piwnica-Worms, *Nat. Med.* **2009**, *15*, 455.
- [26] J.-C. Tseng, A. L. Kung, *Chem. Biol.* **2012**, *19*, 1199.
- [27] X. Chen, H. J. Corbett, S. R. Yukiko, A. P. Raphael, E. J. Fairmaid, T. W. Prow, L. E. Brown, G. J. P. Fernando, M. A. F. Kendall, *Adv. Funct. Mater.* **2011**, *21*, 464.
- [28] D. G. Koutsonanos, E. V. Vassilieva, A. Stavropoulou, V. G. Zarnitsyn, E. S. Esser, M. T. Taherbhai, M. R. Prausnitz, R. W. Compans, I. Skountzou, *Sci. Rep.* **2012**, *2*, 357.
- [29] K. Numata, D. L. Kaplan, *Adv. Drug Delivery Rev.* **2010**, *62*, 1497.
- [30] M.-C. Chen, S.-F. Huang, K.-Y. Lai, M.-H. Ling, *Biomaterials* **2013**, *34*, 3077.
- [31] F. O. Nestle, M. P. Di, J.-Z. Qin, B. J. Nickoloff, *Nat. Rev. Immunol.* **2009**, *9*, 679.
- [32] R. E. Lanford, Z. Feng, D. Chavez, B. Guerra, K. M. Brasky, Y. Zhou, D. Yamane, A. S. Perelson, C. M. Walker, S. M. Lemon, *Proc. Natl. Acad. Sci. U.S.A.* **2011**, *108*, 11223.
- [33] B. Levine, J. M. Hardwick, B. D. Trapp, T. O. Crawford, R. C. Bollinger, D. E. Griffin, *Science* **1991**, *254*, 856.
- [34] D. L. Woodland, J. E. Kohlmeier, *Nat. Rev. Immunol.* **2009**, *9*, 153.
- [35] D. Gray, *Nat. Rev. Immunol.* **2002**, *2*, 60.
- [36] S. N. Mueller, R. Ahmed, *Proc. Natl. Acad. Sci. U.S.A.* **2009**, *106*, 8623.